LBNL-39243
UC-405
Preprint

ERNEST ORLANDO LAWRENCE
BERKELEY NATIONAL LABORATORY

From High Energy Physics to Low Level Vision

N. Sochen, R. Kimmel, and R. Malladi
Physics Division
Mathematics Department

August 1996
To be submitted
for publication

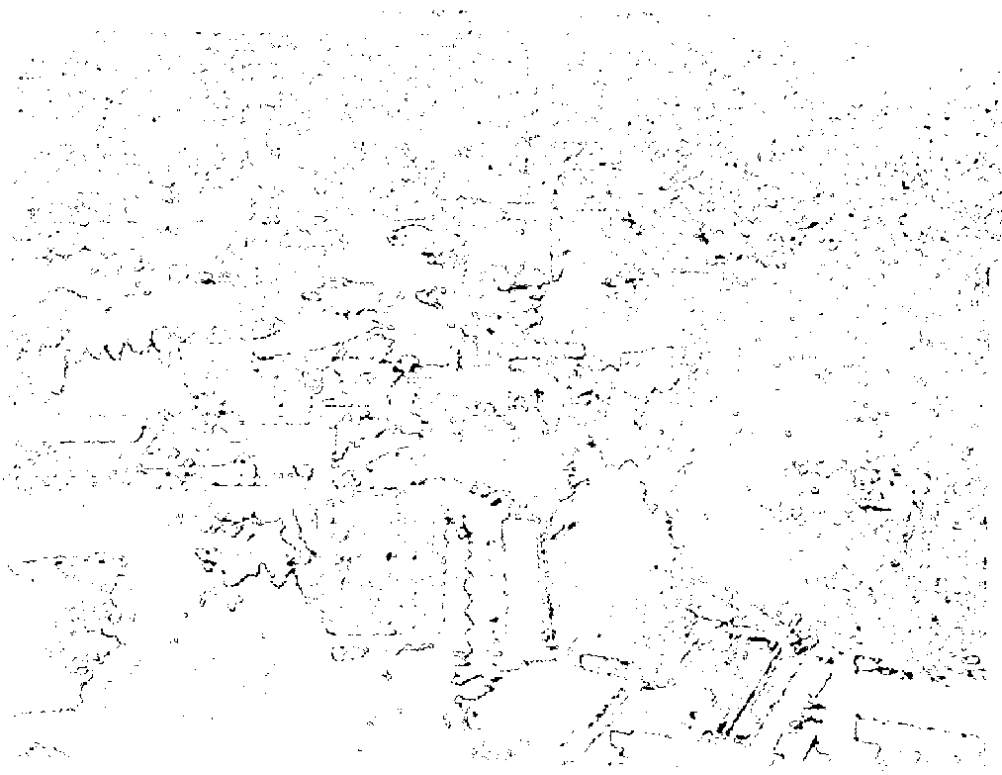

DISCLAIMER

LBL-39243
UC-405

From High Energy Physics to Low Level Vision

N. Sochen,* R. Kimmel,† and R. Malladi†

Physics Division
Ernest Orlando Lawrence Berkeley National Laboratory
University of California
Berkeley, California 94720

August 1996

*Physics Department, University of California, Berkeley.
†Mathematics Department.

This work was supported in part by the Applied Mathematical Sciences subprogram of the Office of Energy Research, U.S. Department of Energy, under Contract No. DE-AC03-76SF00098.

From High Energy Physics to Low Level Vision *

N. Sochen** **R. Kimmel** **R. Malladi**
Lawrence Berkeley National Laboratory
University of California
Berkeley, CA 94720.

Abstract

Based on recent results in high energy physics, a natural flow for image scale space, enhancement, and segmentation is presented. We consider intensity images as surfaces in the $(\mathbf{x}, \mathbf{I})$ space. The image is thereby a 2D surface in 3D space for gray level images, and a 2D surface in 5D for color images. The new formulation unifies many classical schemes and algorithms via a simple scaling of the intensity contrast, and results in new and efficient schemes. Extensions to multi dimensional signals become natural and lead to powerful denoising and scale space algorithms. Here, we demonstrate the proposed framework by applying it to improve the Yanovitz-Bruckstein segmentation method and to denoise color images.

1 Introduction: A philosophical point of view

In the field of high energy physics, scientists try to link between many physical phenomena via a mathematical framework that is as simple as possible. In particular, gravity, which is the theory that describes the dynamics of the geometry of our world is difficult to reconcile with quantum mechanics and with other forces of nature. *String theory*, which is the theory of fluctuating membranes embedded in space-time, emerged in the last 15 years as a promising solution to this problem [22]. In a very similar manner, the importance of the dynamics of the image geometry in the perception and understanding of images is by now well established in computer vision. We will try to link between these two fields through a simple example where an action potential that was recently introduced in string theory is used to produce a natural scale space for images as surfaces in their embedding space. It will lead us to the construction of image enhancement procedures for gray and color images, and to *cartoon* like segmentation [31], and binarization algorithms. This model also links between many existing segmentation and scale space procedures by a change of a single parameter that switches between the definition of norms.

We follow the presentation and philosophical approach of Alvarez and Morel [3], while we differ in the proposed mathematical framework. Alvarez and Morel define the computer

*Report, LBNL-39243, August 1996, Submitted to IEEE Trans. on Image Proc., Aug. 20, 1996
**Physics Department, UC, Berkeley

vision field as follows: *"Computer vision is a branch of science that tries to answer the philosophical, psychological, physiological and technical question: How can the local brightness information arriving at the retina (or to any optical sensor) be transformed into a global percept of the objects, with their distance, color and shape?"* Joint effort in computer vision and psychophysics research in the 60's and 70's [30], suggested that in the first milliseconds of the perception process, there exists a series of parallel, fast, and irreversible operations applied to the retina information and yield rich and useful information to further understand the "image". This is shown to be automated, reflex process, that does not depend on any learning, and is called *low-level vision.*

Low level vision, in a deterministic way, is an input and output process. We will try, in what follows, to understand this process from a mathematical point of view without worrying about the way it is physically implemented in the retina and the brain. Input to the low level vision process is a map $X : \Sigma \to M$ where Σ is a one, two, or three dimensional manifold and X is the embedding of this manifold in a space which is a hybrid space of spatial coordinates and feature coordinates, the "space-feature". For example, the most common map is from a two dimensional surface to $\mathbb{R}^3$ where we have at each point of the plane an intensity $I(x, y)$. The $\mathbb{R}^3$ space-feature has Cartesian coordinates (x, y, I) where x and y are the spatial coordinates and I is the feature coordinate. Higher dimensions of the embedding space are encountered for example in color images. Three dimensional manifolds Σ occur in movie analysis and in medical solid images. Output of the low level process in most models consists of

- A smoothed image from which reliable features can be extracted by local, and therefore differential, operators.

- A segmentation, that is, either a decomposition of the image domain into homogeneous regions with boundaries, or a set of boundary points – an "edge map".

The algorithm supposes the existence of layers serving as operators such that the information is processed locally in the layers and forward to the next layer with no interaction between distance layers. This means that the output has the form $X(\Sigma, t)$ which is the solution of $\partial_t X = OX$ with O a local differential operator. This process is called *scale space* where t is the scale parameter.

There are many definitions for scale space of images aiming to arrive at a coherent framework that unifies many requirements. One such requirement is that *"only isophotes matter"*, or equivalently assume the importance of the *morphological assumption* of the scale space to be *contrast invariant.* We argue that this assumption, though leading to many interesting results, seem to fail in many other natural cases. Let us demonstrate it with a very simple example: Consider the intensity image of a dark object in a white background. At this point the boundary of the object is closely related to one of the isophotes of the gray level image. Consider the intensity image as a function, and add to this function a new smooth function (e.g. a tilted plane). This additional smooth function might be the result of non-uniform lighting conditions. It is obvious that in the new intensity image the isophotes play only a minor role in the understanding process. Actually, the moment we define edges to be related to the gradient of the intensity image in any sense, we break the

morphological assumption and link between the isophotes. To overcome the above problem, a linear assumption was added to the scale space as an optional requirement [3]. However, it imposes heavy constraints on the problem and interfered with the purity and integrity of the mathematical frameworks developed thus far.

The importance of edges that are obtained from the intensity gradient is acknowledged, and gradient based edge detectors are a basic operation in many computer vision applications. Edge detectors appear by now in almost all image processing tools. The importance of edges in scale space construction is also obvious. We argue that boundaries between objects should survive as long as possible along the scale space, while homogeneous regions should be simplified and flattened in a more rapid way. On the other hand, we still want to preserve the geometry and mathematical integrity that result in some interesting non-linear 'scale spaces' as a result of the morphological assumption. Among these are the Euclidean and affine invariant flows [1, 2, 44]. Another important question, for which there are only partial answers, is how to treat multi valued images. A color image is a good example since we actually talk about 3 images (Red, Green, Blue) that are composed into one. Should one treat such images as multi valued functions as proposed in [15]?

We attempt to answer some of the above questions by viewing images as embedding maps, that flow towards minimal surfaces. We go two dimensions higher than most of the classical schemes, and instead of dealing with isophotes as planar curves we deal with the whole image as a surface. For example, a gray level image is no longer considered as a function but as a two dimensional surface in three dimensional space. This idea is quite old [23] for gray level images, yet, to the best of our knowledge, it was never carried on to higher dimensions. As another example, we will consider a color image as a 2D surface now in 5D.

We have chosen to present our ideas in the following order: Section 2 introduces basic concepts in differential Riemannian geometry, where the most important issue is the arclength and the definition of a metric on a surface. Next, Section 3 presents the "action" that we borrowed from high energy physics and the way it produces a general framework for non-linear diffusion in computer vision. Then, in Section 4 we refer to other models that are the result of the same action through different choices of the metric, and we study the geometrical properties of a generalized version of the mean curvature flow that is closely related to the proposed framework. In Section 5 we introduce the flow itself that we have chosen to name *Beltrami flow*, and present a geometric interpretation in the simplest 3D case. Next, Section 6 presents the resulting flow for color images and its relation to previous models. Finally we conclude with two examples: Section 7, uses the proposed framework to introduce a new binarization method for gray level images. Section 8 shows some experiments with color images with and without constraints.

2 Differential Riemannian geometry preliminaries

This section serves as a reminder of Riemannian differential geometry and used to fix the conventions and the terminology needed for our formulation. While we tried to make it accessible to as wide an audience as possible it will be presumptuous of us to present this section as a self contained tutorial. For this purpose we recommend the excellent books of Eisenhart [17], Guggenheimer [24], Dubrovin Fomenko and Novikov [16]. The last reference

as well as the book of Nakahara [33] are more oriented to physics. Nevertheless, we find the exposition of ideas in these books appealing, and we follow the logic and exposition of the chapter on Riemannian geometry in Nakahara's book in the rest of this section.

2.1 The metric

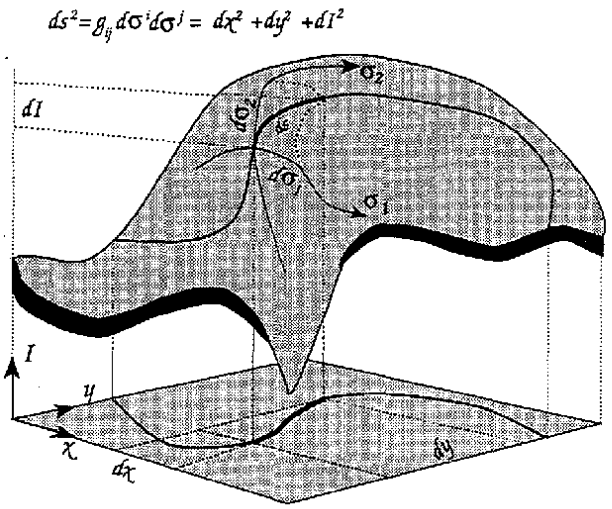

Figure 1: Length element of a surface curve ds, may be defined either as a function of a local metric defined on the surface $(\sigma_1, \sigma_2, (g_{ij}))$, or as a function of the coordinates of the space in which the surface is embedded (x, y, I).

The basic concept of Riemannian differential geometry is distance. The natural question in this context is how do we measure distances? We will first take the important example $X : \Sigma \to \mathbb{R}^3$. We denote the local coordinates on the two dimensional manifold Σ by (σ^1, σ^2), these are the analog of the arc length for the one dimensional manifold, i.e. a curve, see Fig. 1. The map X is explicitly given by $(X^1(\sigma^1, \sigma^2), X^2(\sigma^1, \sigma^2), X^3(\sigma^1, \sigma^2))$. Since the local coordinates σ^i are curvilinear, and not orthogonal in general, the distance square between two close points on Σ, $p = (\sigma^1, \sigma^2)$ and $p + (d\sigma^1, d\sigma^2)$ is not $ds^2 = d\sigma_1^2 + d\sigma_2^2$. In fact, the squared distance is given by a positive definite symmetric bilinear form $g_{ij}(\sigma^1, \sigma^2)$ called the metric

$$ds^2 = g_{\mu\nu} d\sigma^\mu d\sigma^\nu \equiv g_{11}(d\sigma^1)^2 + 2g_{12} d\sigma^1 d\sigma^2 + g_{22}(d\sigma^2)^2, \tag{1}$$

where we used Einstein summation convention in the second equality; identical indices that appear one up and one down are summed over. We will denote the inverse of the metric by $g^{\mu\nu}$, so that $g^{\mu\nu} g_{\nu\gamma} = \delta^\mu_\gamma$, where δ^μ_γ is the Kronecker delta. The metric defines naturally an inner product: $(V, W) \equiv g_{ij} V^i W^j$ where V and W are two vectors fields on Σ.

2.2 Induced metric

Let $X : \Sigma \to M$ be an embedding of Σ in M, where M is a Riemannian manifold with a metric $(g_{ij})_M$. We can use the knowledge of the metric on M and the map X to construct the metric on Σ. This procedure, which is denoted formally as $(g_{\mu\nu})_\Sigma = X^*(g_{ij})_M$, is called the *pullback* for obvious reasons and is given explicitly as follow:

$$(g_{\mu\nu})_\Sigma(\sigma^1, \sigma^2) = (g_{ij})_M(X(\sigma^1, \sigma^2))\partial_\mu X^i \partial_\nu X^j, \tag{2}$$

where $i, j = 1, ..., \dim M$ are being summed over, and in short we use

$$\partial_\mu X^i \equiv \frac{\partial X^i(\sigma^1, \sigma^2)}{\partial \sigma^\mu}.$$

Example: The two sphere S^2 embedded in $\mathbb{R}^3$.
The embedding is the usual one, with the local coordinates $(\sigma^1, \sigma^2) \equiv (\theta, \psi)$ and a map:

$$X : (\theta, \psi) \to (sin\theta \cos\psi, \sin\theta \sin\psi, \cos\theta). \tag{3}$$

The metric of $\mathbb{R}^3$ in Cartesian coordinate system is the Kronecker delta δ_{ij}. With the map X and the metric of $\mathbb{R}^3$ we can use the above formula to get the induced metric:

$$\begin{aligned} ds^2 &= g_{\mu\nu} d\sigma^\mu d\sigma^\nu \\ &= \delta_{ij}\partial_\mu X^i \partial_\nu X^j d\sigma^\mu d\sigma^\nu \\ &= A d\theta d\theta + 2B d\theta d\psi + C d\psi d\psi, \end{aligned} \tag{4}$$

where

$$A = 1, \qquad B = 0, \qquad C = \sin^2\theta. \tag{5}$$

Let us calculate C for example:

$$\begin{aligned} C &= (\partial_\psi(\sin\theta\cos\psi))^2 + (\partial_\psi(\sin\theta\sin\psi))^2 + (\partial_\psi(cos\theta))^2 \\ &= (\sin\theta\sin\psi)^2 + (-\sin\theta\cos\psi)^2 + 0 \\ &= \sin^2\theta. \end{aligned} \tag{6}$$

A and B are calculated in a similar manner.

The second example which is often used in computer vision is the embedding of a surface described as a graph in $\mathbb{R}^3$:

$$X : (\sigma^1, \sigma^2) \to (\sigma^1, \sigma^2, I(\sigma^1, \sigma^2)). \tag{7}$$

Using Equation (2) we get

$$(g_{\mu\nu}) = \begin{pmatrix} 1 + I_x^2 & I_x I_y \\ I_x I_y & 1 + I_y^2 \end{pmatrix} \tag{8}$$

where we used the identification $X \equiv \sigma^1$ and $Y \equiv \sigma^2$ in the map X.

Actually we can understand this result in an intuitive way: Eq. (2) means that the distance measured on the surface by the local coordinates is equal to the distance measured in the embedding coordinates, see Figure 1. Under the above identification, we can write

$$\begin{aligned} ds^2 &= dx^2 + dy^2 + dI^2 \\ &= dx^2 + dy^2 + (I_x dx + I_y dy)^2 \\ &= (1 + I_x^2)dx^2 + 2I_x I_y dx dy + (1 + I_y^2)dy^2. \end{aligned}$$

2.3 Parallel transport

In order the take derivatives of a vector field on a manifold we need to compare vectors at different points on the manifold. This is obvious from the heuristic formula

$$\frac{\partial V^i}{\partial x^j} = \lim_{\Delta x \to 0} \frac{V^i(..., x^j + \Delta x^j, ...) - V^i(..., x^j, ...)}{\Delta x^j} . \tag{9}$$

We see that the first term in the numerator is defined at $x + \Delta x^j$ while the second term is defined at x. In order to have a meaningful expression we have to transport $V^i(x)$ to $x + \Delta x^j$ *without change* and compute the difference. Since there is no natural way, in general, to do that, we have to specify how we perform this procedure which is called **parallel transport**. Let $\tilde{V}|_{x+\Delta x}$ denote a vector $V|_x$ parallel transported to $x + \Delta x$. We demand that the components $\tilde{V}^i$ satisfy
$\tilde{V}^i(x+\Delta x) - V^i(x) \propto \Delta x$,
$\widetilde{(V^i + W^i)}\,(x+\Delta x) = \tilde{V}^i(x+\Delta x) + \tilde{W}^i(x+\Delta x)$.

These conditions are satisfied if we take

$$\tilde{V}^i(x + \Delta x) = V^i(x) - V^k(x)\Gamma^i_{jk}\Delta x^j \tag{10}$$

and the covariant derivative with respect to x^j is defined as

$$\lim_{\Delta x \to 0} \frac{V^i(..., x^j + \Delta x^j, ...) - \tilde{V}^i(..., x^j, ...)}{\Delta x^j} = \frac{\partial V^i}{\partial x^j} + \Gamma^i_{jk} V^k. \tag{11}$$

Different choices of Γ^i_{jk} correspond to different ways to parallel transport.

2.4 Geodesics

Another way to understand the connection coefficients Γ^i_{jk} is the following: Vector fields components are given at any point on the manifold in terms of the local frame. In general, frames at different point of the manifold are different. The connection describes how the frame is changed infinitesimally on the manifold. Denote the basis vectors of the local frame by e_μ, we can take for example the directions along the local coordinates $e^\mu = \partial/\partial\sigma^\mu$. Denote the covariant derivative by $\mathcal{D}$, then the change of the frame when moved infinitesimally to one of the vector basis directions is

$$\mathcal{D}_\mu e_\nu = \mathcal{D}_{e_\mu} e_\nu = e_\gamma \Gamma^\gamma_{\mu\nu}. \tag{12}$$

Similarly, moving one vector in the direction of another vector is

$$\begin{aligned} \mathcal{D}_V W &= V^\mu \mathcal{D}_{e_\mu}(W^\nu e_\nu) = V^\mu (e_\mu[W^\nu] e_\nu + W^\nu \mathcal{D}_{e_\mu} e_\nu) \\ &= V^\mu (\partial W^\gamma/\partial\sigma^\mu + W^\nu \Gamma^\gamma_{\mu\nu}) e_\gamma. \end{aligned}$$

Let now Σ be an interval $\mathcal{I} = (a, b)$ and M some Riemannian manifold. The map $\mathcal{C} : \mathcal{I} \to M$ is a curve on M. Let W be a vector field along the curve and V the tangent vector to the curve

$$V = \frac{d}{ds} = (\frac{dX^i(t)}{ds})e_i. \tag{13}$$

If W satisfies

$$\mathcal{D}_V W = 0 \qquad \text{for any } s \in (a, b), \tag{14}$$

then W is said to be parallel transported along $\mathcal{C}(s)$. If the tangent vector itself is parallel transported along the curve $\mathcal{C}$, that is, if

$$\mathcal{D}_V V = 0, \tag{15}$$

then the curve $\mathcal{C}(s)$ is called a **geodesic**. In components, this equation reads

$$\frac{d^2X^i}{ds^2} + \Gamma^i_{jk}\frac{dX^j}{ds}\frac{dX^k}{ds} = 0, \tag{16}$$

where X^i are the coordinates of $\mathcal{C}(s)$.

2.5 The Levi-Civita Connection

The connection up to this point was arbitrary. We will now choose a special connection by adding a condition on the space of connections. Remember that the metric defines an inner product on the manifold. We demand that if two vectors X and Y are parallel transported along any curve on the manifold then the inner product between them remains constant under parallel transport. Let V be a tangent vector to some curve along which the vectors X and Y are parallel transported, then

$$\mathcal{D}_V(g_{ij}X^iY^j) = V^k\mathcal{D}_k(g)_{ij}X^iY^j, \tag{17}$$

where we used the fact that X and Y are parallel transported $\mathcal{D}_V X = \mathcal{D}_V Y = 0$. Since X, Y and V are arbitrary we must have

$$\mathcal{D}_k(g)_{ij} = 0. \tag{18}$$

A connection that satisfies this condition is called *metric compatible.* At this point we will quote the result:

Theorem 1 (The fundamental theorem of Riemannian geometry) *On a Riemannian manifold (M, g) there exist a unique symmetric connection which is compatible with the metric g. This connection is called the* **Levi-Civita Connection** *and the components are given by the following expression*

$$\Gamma^i_{jk} = \frac{1}{2}g^{il}(\partial_j g_{lk} + \partial_k g_{jl} - \partial_l g_{jk}). \tag{19}$$

3 Polyakov Action and Harmonic Maps

In this section, we present a general framework for non-linear diffusion in computer vision. We will show that many of the known methods fall naturally into this framework and how to derive new ones. The equations will be derived by a minimization problem from an action functional. The functional in question depends on *both* the image manifold and the embedding space. Denote by (Σ, g) the image manifold and its metric and by (M, h) the space-feature manifold and its metric, then the map $X : \Sigma \to M$ has the following weight

$$S[X^i, g_{\mu\nu}, h_{ij}] = \int d^m\sigma \sqrt{g} g^{\mu\nu} \partial_\mu X^i \partial_\nu X^j h_{ij}(X), \tag{20}$$

where m is the dimension of Σ, g is the determinant of the image metric, $g^{\mu\nu}$ is the inverse of the image metric, the range of indices is $\mu, \nu = 1, \ldots, \dim \Sigma$, and $i, j = 1, \ldots, \dim M$, and h_{ij} is the metric of the embedding space.

This functional, for $m = 2$, was first proposed, to the best of our knowledge, by Polyakov [38] in the context of high energy physics, and the theory is known as *string theory*. The proposal is to replace the usual picture of a point particle moving in space-time, a motion that describes a curve, by a fundamental string for which the motion in time describes an embedding of a surface in space-time. String theory is the most promising candidate to solve the problem of quantum gravity and the unification of all forces of nature. As we show, it plays a natural role in computer vision as well.

Given the above functional, we have to choose the minimization. We may choose for example to minimize with respect to the embedding alone. In this case the metric $g_{\mu\nu}$ is treated as a parameter of the theory and may be fixed by hand. Another choice is to vary only with respect to the feature coordinates of the embedding space, or we may choose to vary the image metric as well. We will see that these different choices yield different flows. Some flows are recognized as existing methods like the heat flow, the Perona-Malik flow, or the mean-curvature flow. Other choices are new and will be described below in detail.

To gain some intuition about this functional, let us take the example of a surface embedded in $\mathbb{R}^3$ and treat both the metric $(g_{\mu\nu})$ and the spatial coordinates of the embedding space as free parameters, and let us fix them to

$$g = \begin{pmatrix} 1 & 0 \\ 0 & 1 \end{pmatrix} \quad , \quad x = \sigma^1 \quad , \quad y = \sigma^2. \tag{21}$$

We also adopt in $\mathbb{R}^3$ the Cartesian coordinates (i.e. $h_{ij} = \delta_{ij}$). Then, up to a non-important constant, we get

$$S[I, g_{\mu\nu} = \delta_{\mu\nu}, h_{ij} = \delta_{ij}] = \int d^2\sigma |\nabla I|^2. \tag{22}$$

If we now minimize with respect to I, we will get the usual heat operator acting on I.

Using standard methods in variation calculus (see Appendix A), the Euler-Lagrange equations with respect to the embedding are:

$$-\frac{1}{2\sqrt{g}}h^{il}\frac{\delta S}{\delta X^l} = \frac{1}{\sqrt{g}}\partial_\mu(\sqrt{g}g^{\mu\nu}\partial_\nu X^i) + \Gamma^i_{jk}\partial_\mu X^j\partial_\nu X^k g^{\mu\nu} = 0. \tag{23}$$

Few remarks are in order. First notice that we used our freedom to multiply the Euler-Lagrange equations by a strictly positive function. Since $(g_{\mu\nu})$ is positive definite, $g \equiv \det(g_{\mu\nu}) > 0$ for all σ^μ. This factor is the simplest one that doesn't change the minimization solution while giving a reparametrization invariant expression. We will see below that the Perona-Malik flow, for example, corresponds to another choice of the pre-factor, namely 1. The operator that is acting on X^i in the first term is the natural generalization of the Laplacian from flat spaces to manifolds and is called *the second order differential parameter of Beltrami* [27], or for short *Beltrami operator*, and we will denote it by Δ_g. When the embedding is in an Euclidean space with Cartesian coordinate system the connection elements are zero.

The Beltrami operator with a metric that corresponds to the plane with non Cartesian coordinate system was discussed in Florac *et al.* [21]. Our approach is a generalization in two ways, one is the choice of a metric with non-trivial Riemann tensor (or equivalently for surfaces, the Gaussian curvature is different from zero), the other is the possibility to deal with non-trivial embedding. We also have here a framework that can treat curves, surfaces, and higher dimensional image data embedded in gray, color and higher dimensional embedding spaces.

The example of a curve is a good one because it will demonstrate the meaning of the Euler-Lagrange equations. Suppose that we have a curve $\mathcal{C}$ embedded in a two dimensional curved manifold – a surface M. The metric in $\mathcal{C}$ is $g = 1$ if we measure distances according to the arclength. The metric on M is h_{ij} and the Euler Lagrange equations are

$$\frac{d^2X^i}{ds^2} + \Gamma^i_{jk}\frac{\partial X^j}{ds}\frac{\partial X^k}{ds} = 0. \tag{24}$$

We recognize this as the geodesic equation (16) which is the minimization solution to the length of a path between two points on the surface.

For a surface Σ, embedded in 3 dimensional Euclidean space, we get a minimal surface as the solution to the minimization problem. In order to see that and to connect to the usual representation of the minimal surface equation, we vary the action with respect to the metric $g_{\mu\nu}$:

$$\frac{1}{\sqrt{g}}\frac{\delta S}{\delta g^{\mu\nu}} = \partial_\mu X^i\partial_\nu X_i - \tfrac{1}{2}g_{\mu\nu}(g^{\gamma\delta}\partial_\gamma X^i\partial_\delta X_i) = 0.$$

This is solved for the metric

$$g_{\mu\nu} = \partial_\mu X^i \partial_\nu X_i. \tag{25}$$

On inspection, this equation is simply the induced metric on Σ, see Eq. (4). For the case of a surface embedded in $\mathbb{R}^3$ with Cartesian coordinate system we calculated it explicitly in Section 2 (see Eq. (8)). Plugging this induced metric in the first Euler-Lagrange equation 23 we get the steepest decent flow

$$\vec{X}_t = H\vec{\mathcal{N}}, \tag{26}$$

where H is the mean curvature, $\vec{\mathcal{N}}$ is the normal to the surface: [1]

$$H = \frac{(1+I_x^2)I_{yy} - 2I_xI_yI_{xy} + (1+I_y^2)I_{xx}}{g^{\frac{3}{2}}} \quad , \quad \vec{\mathcal{N}} = \frac{1}{\sqrt{g}}(-I_y, -I_x, 1)^T \tag{27}$$

and $g = 1 + I_x^2 + I_y^2$. We see that this choice gives us the mean curvature flow! This should not be a surprise, since if we check how this choice effects the action functional, we notice that, for this choice of metric $g_{\mu\nu}$, we are left with

$$S = \int d^2\sigma\sqrt{g} = \int d^2\sigma\sqrt{\det(\partial_\mu X^i \partial_\nu X_i)},$$

which is the Euler functional that describes the area of the surface (also known in high energy physics as the Nambu action).

In general for any manifold Σ and M, the map $X : \Sigma \to M$ that minimizes the action S with respect to the embedding is called a **harmonic map**. The harmonic map is the natural generalization of the geodesic curve and the minimal surface to higher dimensional manifolds and for different embedding spaces.

4 Choices that Lead to Known Methods

We will survey in this section different choices for the dynamic and parametric degrees of freedom in the action functional.

[1] In what follows, we denote by g the determinant of the metric, $g \equiv \det(g)$, the metric itself will be denoted as (g_{ij}). Note also that some definitions of the mean-curvature include a factor of 2 that we omit in our definition.

4.1 Linear scale-space

Recently, Florac *et al.* [20] invoked parameterization invariance in vision. The basic motivation in their work is to give a formulation of the linear scale-space, which is based on the linear heat flow, that lends itself to treatment in different coordinate systems. As an application, they present the explicit form of the flow for the log-polar coordinate system, which is of special interest due to indications that this is the coordinate system implemented in the brain. Florac *et al.* [20] also noted on the possibility to use a non flat metric, and raised the idea of using an image induced metric.

In order to have parameterization invariance one has to write an invariant differential operator which is the Beltrami operator. The major difference then between our approach and the one given in [20] is the class of metrics allowed. Since a change in parameterization can not change the geometry of the problem, and since they are interested in a linear scale-space, they only allow metrics for which the Riemann tensor vanishes, that is metrics of a flat space.

Our point of view is that an image is a surface embedded in $\mathbb{R}^n$ (or a more general Riemannian manifold). From this perspective the natural metric to choose is the induced metric of the surface. This metric is never flat for a significant image. We discuss these flows below. Other choices of the metric, which are different from both the metric that correspond to a flat space and the induced metric are presented in the next subsection.

4.2 Perona-Malik flow in n dimensions

We fix, as in the linear case, the xy coordinates and vary the action with respect to I while the metric is arbitrary for the time being. Using the Euler-Lagrange equation without any pre-factor, we get the following flow

$$I_t = \partial_\mu \sqrt{g} g^{\mu\nu} \partial_\nu I.$$

We assume now that the image is an n dimensional manifold embedded in $\mathbb{R}^{n+1}$. The task at hand is to find the right choice of the metric to reproduce the Perona-Malik flow. We select $(g_{\mu\nu}) = \tilde{f}\mathcal{I}_d$, where $\mathcal{I}_d$ is the identity matrix. The determinant is $g = (\tilde{f})^n$, and consequently the flow is

$$I_t = \sum_{\mu=1}^{n} \partial_\mu \tilde{f}^{\frac{n}{2}-1} \partial_\mu I.$$

For any dimension different from two we can choose $\tilde{f}^{\frac{n}{2}-1} = C(I)$ to get

$$I_t = \mathrm{div}\,(C(I)\nabla I),$$

which is the basic idea of Perona and Malik [36, 37]. If we further specify $\tilde{f}^{\frac{n}{2}-1} = C(I) = \frac{f(I_0)}{|\nabla I|}$, where I_0 is the original image, we arrive at

$$I_t = \mathrm{div}\left(f(I_0)\frac{\nabla I}{|\nabla I|}\right),$$

which is the core (up to the $|\nabla I|$ normalization factor) of what is known in the literature as the geodesic active contours [6, 7, 45, 25]. Note that this works only for dimension different from two. Examples for higher dimensional manifolds in vision and image processing are 3D images and movies as 3 dimensional manifolds, 3D movie as 4D manifold etc. The Perona-Malik flow in 2 dimension does not fit into this framework. We should note, though, that our flow is in some sense a natural generalization of the Perona-Malik idea since what we have actually, in the natural coordinate system were we identify $(x, y) = (\sigma^1, \sigma^2)$, is

$$I_t = f(I_x, I_y)(\partial_x(C_1 I_x) + \partial_x(C_2 I_y) + \partial_y(C_3 I_x) + \partial_y(C_4 I_y)).$$

The Perona-Malik flow corresponds to the choice $f = 1$, $C_1 = C_4 = C$ and $C_2 = C_3 = 0$. Our approach gives the C_i's and the f a special form which has a well define geometrical meaning and it is derived from a minimization of an action functional.

4.3 The mean curvature flow

In this subsection we choose to minimize with respect to all the available variables in the action. We will also comment below on the different, and equivalent, definitions of the mean curvature. Some of them lend themselves towards natural generalizations.

Going back to the action (20) and minimizing each one of the embedding coordinates X^i, and with respect to the metric $g_{\mu\nu}$, we get the Euler Lagrange equations (see the derivation of these equations in Appendix A):

$$\begin{aligned} \frac{1}{\sqrt{g}}\partial_\mu(\sqrt{g}g^{\mu\nu}\partial_\nu X^i) + \Gamma^i_{jk}\partial_\mu X^j \partial_\nu X^k g^{\mu\nu} &= 0, \\ \partial_\mu X^i \partial_\nu X_i - \frac{1}{2}g_{\mu\nu}(g^{\gamma\delta}\partial_\gamma X^i \partial_\delta X^j h_{ij}) &= 0. \end{aligned} \tag{28}$$

Solving the second equation for the metric we conclude that the minimizing metric is the induced metric

$$(g_{\mu\nu}) = \begin{pmatrix} 1+I_x^2 & I_x I_y \\ I_x I_y & 1+I_y^2 \end{pmatrix}, \tag{29}$$

as one can check easily by substituting this solution back in the second equation of the Euler-Lagrange (28), and use the fact that

$$g^{\gamma\delta}g_{\gamma\delta} = \delta^\gamma_\gamma = 2.$$

Substituting the induced metric in the minimizing equation for the embedding coordinates and identifying $(x, y) = (\sigma^1, \sigma^2)$ we get the mean curvature flow

$$\vec{X}_t = H\vec{\mathcal{N}}, \tag{30}$$

where H, $\vec{\mathcal{N}}$ are given in Eq. (27).

The geometrical meaning of this flow is evident. Each point of the surface moves in the direction of the normal with velocity proportional to the mean curvature.

Before closing this subsection we briefly discuss the different formulations and equivalent definitions of the mean curvature. The standard definition is through the two principal curvatures k_1 and k_2. Denote the mean curvature by H then

$$H = k_1 + k_2. \tag{31}$$

where k_i are the principle curvatures. An equivalent way is to define the mean curvature as a trace of the second fundamental form. Although the 2×2 matrix of the second fundamental form depends on the coordinate system used, the trace is invariant under similarity transformation and describes a geometrical quantity – the mean curvature. The second fundamental form is defined from both intrinsic information of the surface and from extrinsic information – the embedding. Of particular importance is the *normal* to the surface. Denote the second fundamental form by $d_{\mu\nu}$, then

$$d_{\mu\nu} = \langle \partial_\mu \partial_\nu X, \vec{\mathcal{N}} \rangle = \sum_{i=1}^{3} \vec{\mathcal{N}}^i \partial_\mu \partial_n u X^i. \tag{32}$$

For our canonical example $X : (\sigma^1, \sigma^2) \to (\sigma^1, \sigma^2, I(\sigma^1, \sigma^2))$ we find that

$$d_{\mu\nu} = \frac{\partial_\mu \partial_\nu I}{\sqrt{g}}. \tag{33}$$

The trace is given by

$$H = g^{\mu\nu} d_{\mu\nu} \tag{34}$$

where μ and ν are summed over. One only needs to check it in one coordinate system since this equation is invariant to general coordinate transformation of the surface. In our canonical coordinate system, for example, we obtain

$$\begin{aligned} g^{\mu\nu} d_{\mu\nu} &= \frac{1}{g^{\frac{3}{2}}} (g_{22} d_{11} - 2 g_{12} d_{12} + g_{11} d_{22}) \\ &= \frac{1}{g^{\frac{3}{2}}} \left((1 + I_y^2) I_{xx} - 2 I_x I_y I_{xy} + (1 + I_x^2) I_{yy} \right) = H. \end{aligned} \tag{35}$$

The generalization to higher dimensions is obvious and known for a long time for the special case of hypersurfaces, that is, embedding with codimension 1. Take an n dimensional manifold, for example, and embed it in $\mathbb{R}^{n+1}$. There is a *unique* normal to this hypersurface which is given by the formula

$$N_i = \epsilon_{ii_1 i_2 \ldots i_n} V_1^{i_1} V_2^{i_1} \cdots V_n^{i_n} \tag{36}$$

where V_i $i = 1, 2, \cdots, n$ are the the basis vectors of the tangent space to the hypersurface, and $\epsilon_{ii_1 \ldots, i_n}$ is the totally antisymmetric tensor. With the normal we can find explicitly the second fundamental form as an $n \times n$ matrix and find the trace. We are guaranteed to find

$$H = g^{\mu\nu} d_{\mu\nu} = k_1 + k_2 + \cdots + k_n. \tag{37}$$

For images which are maps from an n dimensional manifold to m dimensional embedding space with $m - n > 1$ the above analysis fails. The normals to the image span an $n - m$ normal space and the second fundamental form is not well defined. The only way, that we can see, to generalize the mean curvature flow to these maps is to use the Beltrami operator. This operator is built from the metric only, and we don't need any extrinsic information to express it. It acts on the embedding coordinates and coincides with the mean curvature for hypersurfaces. We call this generalized flow the *Beltrami flow* and discuss its characteristics in the next section.

5 The Beltrami flow

We present in this section a new and natural flow. The image is regarded as an embedding map $X : \Sigma \to \mathbb{R}^3$, where Σ is a two dimensional manifold, and the flow is natural in the sense that it minimizes the action functional with respect to I and (g_{ij}), while being reparametrization invariant. The coordinates X and Y are parameters from this view point and are identified as above with σ^1 and σ^2 respectively. The result of the minimization is the Beltrami operator acting on I:

$$I_t = \Delta_g I \equiv \frac{1}{\sqrt{g}} \partial_\mu (\sqrt{g} g^{\mu\nu} \partial_\nu I) = H \vec{\mathcal{N}}_{\hat{I}} \tag{38}$$

where the metric is the induced one given in Eq. 2, and $\hat{I}$ is the unit vector in the I direction.

The geometrical meaning is obvious. Each point on the image surface moves with a velocity that depends on the mean curvature and the I component of the normal to the surface at that point. Since along the edges the normal to the surface lie almost entirely in the X-Y plane, I hardly changes along the edges while the flow drives other regions of the image towards a minimal surface at a more rapid rate. Let us further explore the geometry of the flow in 3D and relate it to other known methods.

5.1 Geometric Flows Towards Minimal Surfaces

A minimal surface is the surface with the least area that satisfies given boundary conditions. It has nice geometrical properties, and is often used as a natural model of various physical phenomena, e.g. soap bubbles 'Plateau's problem", in computer aided design, in architecture (structural design), and recently even for medical imaging [8]. It was realized by J. L. Lagrange in 1762 [28], that the mean curvature equal to zero is the Euler Lagrange equation for area minimization. Hence, the mean curvature flow is the most efficient flow towards a minimal surface. Numerical schemes for the mean curvature flow, and the construction of minimal surfaces under constraints, where introduced since the beginning of the modern age of numerical analysis [14], and is still the subject of ongoing numerical research [12, 13, 10].

For constructing the mean curvature flow of the image as a surface, we follow three steps:

1. Given the surface $\mathcal{S}$ that evolves according to the geometric flow

$$\frac{\partial \mathcal{S}}{\partial t} = \vec{F}, \tag{39}$$

where $\vec{F}$ is an arbitrary smooth flow field. The geometric deformation of $\mathcal{S}$ may be equivalently written as

$$\frac{\partial \mathcal{S}}{\partial t} = \langle \vec{F}, \vec{\mathcal{N}} \rangle \vec{\mathcal{N}}, \tag{40}$$

where $\vec{\mathcal{N}}$ is the unit normal of the surface at each point, and $\langle \vec{F}, \vec{\mathcal{N}} \rangle$ is the inner product (the projection of $\vec{F}$ on $\vec{\mathcal{N}}$). The tangential component affects only the internal parameterization of the evolving surface and does not influence its geometric shape.

2. The mean curvature flow is given by:

$$\frac{\partial \mathcal{S}}{\partial t} = H\vec{\mathcal{N}}, \tag{41}$$

where H is the mean curvature of $\mathcal{S}$ at every point. Let us use the relation given in Step 1:

3. Considering the image function $I(x, y)$, as a parameterized surface $\mathcal{S} = (x, y, I(x, y))$. We may write the mean curvature flow as:

$$\frac{\partial \mathcal{S}}{\partial t} = \frac{H}{\langle \vec{\mathcal{N}}, \vec{Z} \rangle} \vec{Z}, \tag{42}$$

for any smooth vector field $\vec{Z}$ defined on the surface. Especially, we may choose $\vec{Z}$ as the $\hat{I}$ direction, i.e. $\vec{Z} = (0,0,1)$. In this case

$$\frac{1}{\langle \vec{\mathcal{N}}, \vec{Z} \rangle} \cdot \vec{Z} = \sqrt{1 + I_x^2 + I_y^2} \cdot (0,0,1) = \sqrt{g}(0,0,1). \tag{43}$$

Fixing the (x,y) parameterization along the flow (i.e. using the fixed x,y plane as the natural parameterization), we have $\mathcal{S}_t = \frac{\partial}{\partial t}(x,y,I(x,y)) = (0,0,I_t(x,y))$. Thus, for tracking the evolving surface, it is enough to evolve I via

$$\frac{\partial I}{\partial t} = H\sqrt{1 + I_x^2 + I_y^2}, \tag{44}$$

where the mean curvature H is given as a function of the image I, see Fig. 2, and Eq. 27.

$$H = \frac{(1 + I_y^2)I_{xx} - 2I_x I_y I_{xy} + (1 + I_x^2)I_{yy}}{(1 + I_x^2 + I_y^2)^{3/2}}. \tag{45}$$

See [11, 12] for the derivation of H (as D.L. Chopp summarizes the original derivation by J.L. Lagrange from 1762), and Eq. (35 in Section 4.3.

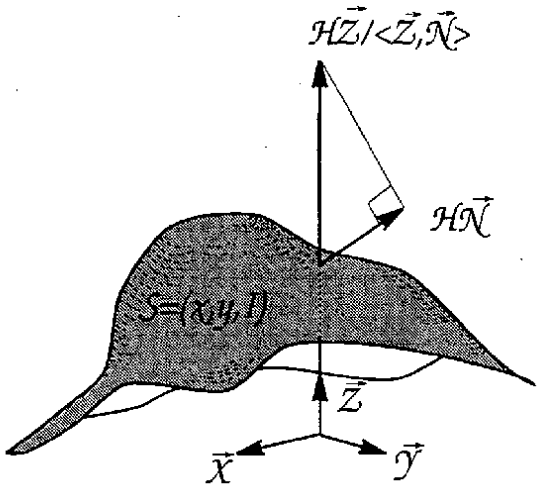

Figure 2: Consider the surface mean curvature flow $\mathcal{S}_t = H\vec{\mathcal{N}}$, mean curvature H in the surface normal direction $\vec{\mathcal{N}}$. A geometrically equivalent flow is the flow $\partial(x,y,I)/\partial t = H(1 + |\nabla I|^2)^{1/2} \cdot (0,0,1)$ which yields the mean curvature flow when projected onto the normal.

We end up with the following evolution equation

$$I_t = \frac{(1+I_y^2)I_{xx} - 2I_xI_yI_{xy} + (1+I_x^2)I_{yy}}{1+I_x^2+I_y^2}, \tag{46}$$

with the image itself as initial condition $I(x,y,0) = I(x,y)$. Using Beltrami second order operator Δ_g and the metric g, Equation (46) may be read as

$$I_t = g\Delta_g I. \tag{47}$$

While the Beltrami flow (selective mean curvature flow) $I_t = \Delta_g I$ is given explicitly for the simple 2D case as

$$I_t = \frac{(1+I_y^2)I_{xx} - 2I_xI_yI_{xy} + (1+I_x^2)I_{yy}}{(1+I_x^2+I_y^2)^2}, \tag{48}$$

see Figure 3.

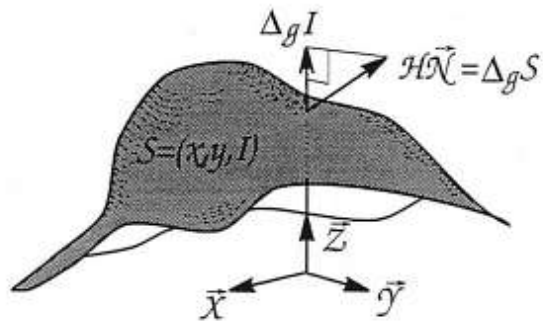

Figure 3: Consider the mean curvature H in the surface normal direction $\vec{\mathcal{N}}$. It can also be expressed as $H\vec{\mathcal{N}} = \Delta_g \mathcal{S}$. Beltrami operator that operates on I: $\Delta_g I$, is the third component of this vector: Projection onto the I ($\vec{Z}$) direction.

5.2 Gray scale: Previous mean curvature flows

In [18], the authors realized that setting the weighting function $c(x,y,t)$ in the Perona-Malik [36] anisotropic diffusion model $I_t = \mathrm{div}(c(x,y,t)\nabla I)$, to $c(x,y,t) = (1+I_x+I_y)^{-1/2}$, the diffusion becomes the mean curvature flow (up to a factor):

$$I_t = H. \tag{49}$$

They presented some nice properties of this flow for gray scale image processing. Their flow is the mean curvature multiplied by the projection of the surface normal onto the I axis. Or

geometrically, they rotate the curvature normal vector so that it coincides with the $\vec{Z}$ axis. We therefore refer to this flow as 'normalized mean curvature flow'. It is located somewhere between the mean curvature flow for the image as a surface $I_t = g\Delta_g I = H\sqrt{g}$ that was used in [29] to denoise images, and our Beltrami flow, which in the 2D case simplifies to $I_t = \Delta_g I = H/\sqrt{g}$. All of these flows lead towards a minimal surface, yet the proposed framework better preserves the edges, and may be naturally extended to any number of dimensions.

Fig. 4 compares between the results of the Beltrami flow and the mean curvature flow both applied to a digital subtraction angiogram (DSA). It demonstrates the edge preserving property of the Beltrami flow relative to the mean curvature flow.

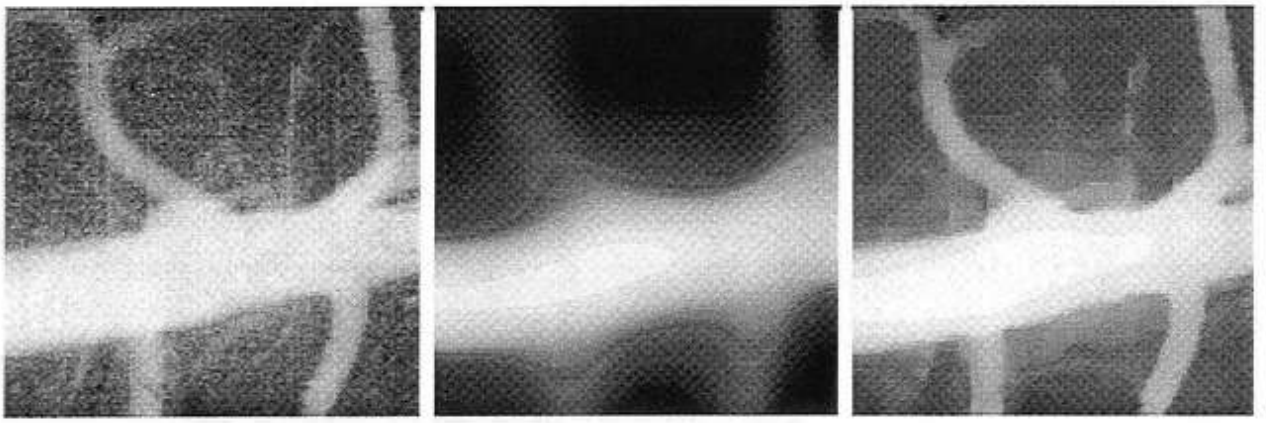

Figure 4: On the left is the original medical image. In the middle is the result of smoothing via the mean curvature flow, and on the right is the result of the Beltrami flow.

We note again that some properties for the mean curvature flows are studied by the PDE community , e.g. [34]. One important result, at least for the level set framework [35], in which the mapping is from $\mathbb{R}^m$ to $\mathbb{R}^{m+1}$ (embedding with codimension 1) is that embedding of evolving surfaces is preserved [19]. Roughly speaking, it means that surfaces can not cross as they evolve if they do not cross to begin with.

5.2.1 Gray scale: Relation to total variation (TV) methods

Let us show the direct relation to TV methods and especially for the regularization introduced by Vogel and Oman [49], and efficiently implemented for changing the regularization ratio (from large to small) in [10]. We will show that by modifying the aspect ratio between the intensity and the xy coordinates we are able to switch between norms. It is possible to obtain the TV norm, travel through minimal surfaces, and end up with potential surfaces at the other limit.

The regularized TV is defined by: $\min \int \sqrt{\beta^2 + |\nabla I|^2}$, where β is a real number, subject to constraints that are used to monitor the drifting of the evolving image from the initial one. Contrast scaling of $I \rightarrow \beta I$, we have $\nabla I \rightarrow \beta \nabla I$ and the TV norm becomes $\int \sqrt{1 + |\nabla I|^2}$. This is exactly an area minimization towards a minimal surface that could be realized through mean curvature flow with the constraints imposed by the noise variance and scale. In other words, the regularized TV is in fact a flow towards a minimal surface with respect to the scaled surface $(x, y, \beta I)$. The ratio between the image size (resolution) and the gray level is taken in an arbitrary way for creating an artificial Euclidean metric, therefore, setting this ratio to β brings us to the minimal surface computation. It is important to note that the β ratio should be determined for every image processing algorithm. The β ratio may be introduced via Polyakov action by defining the embedding space to be

$$(h_{ij}) = \begin{pmatrix} 1 & 0 & 0 \\ 0 & 1 & 0 \\ 0 & 0 & \beta^2 \end{pmatrix}. \tag{50}$$

The only way to avoid the β ratio dependence is to construct planar curve evolution for the gray level sets, such that embedding is preserved [2, 1, 44, 26]. This was called 'contrast invariance' in [3]. Yet, these schemes are pure smoothing schemes that do not preserve edges.

We note that it is possible to impose constraints on the functional that modify the flow like the variance constraints of the Rudin-Osher-Fatemi total variation (TV) method [40]. Two such constraints are introduced in Appendix B for the color case.

We note that the Rudin-Osher-Fatemi TV model [40] minimizes $\int |\nabla I|$, while the Blake and Zisserman membrane model [4] minimizes $\int |\nabla I|^2$ (up to the constraints). The TV, minimal surfaces (invariant membrane), and potential surfaces are all obtained from different scalings of the β ratio. A potential surface ($\Delta I = 0$), is a specific case of a minimal surface for which the ratio parameter β is taken to be large, i.e. $|\nabla I|$ is relatively small. These kind of surfaces are often used in the segmentation context, e.g. [39, 32]. Since the aspect ratio of the I axis with respect to the x and y axis is taken arbitrarily, one could select it relatively large, so that the result is close to a potential surface. The 2D surface area minimization model is closely related to the invariant membrane of Blake and Zisserman [4] (up to the constraints). Actually, Blake and Zisserman noticed that there is a link between the invariant membrane and the non invariant membrane models. Where this link is the aspect ratio of the gray level and the xy coordinates: *"The invariant energy is well approximated by the non invariant one provided $|\nabla I|$ is small enough. Thus, for small signals, the invariant membrane acts like the non-invariant one"* [4], page 93.

In a similar spirit, Grimson's method [23] and its computation method as described in [4], page 25: *"an elaboration of a simple 'relaxation' algorithm that computes the shape of*

a soap film by repeated averaging", is related to the idea of decreasing the β ratio of the regularized TV method as addressed in [10]. Thereby, a natural way to further improve the efficiency of the TV method is to use multi-grid techniques, the same way Terzopoulos used such techniques to improve the efficiency of his extensions to Grimson's method in [46].

We have just shown that large β ratio leads to potential surfaces, while at small ratio we have the TV norm. We have thereby linked together many classical schemes via a selection of one parameter, that is, the image gray level scale with respect to its xy coordinates. This scale is determined arbitrarily anyhow in most of the current schemes.

6 Color

We generalize the Beltrami flow to the 5 dimensional space-feature needed in color images. The embedding space-feature space is taken to be Euclidean with Cartesian coordinate system. The image, thus, is the map $f : \Sigma \rightarrow \mathbb{R}^5$ where Σ is a two dimensional manifold. Explicitly the map is

$$f = \left(X(\sigma^1,\sigma^2), Y(\sigma^1,\sigma^2), I^r(\sigma^1,\sigma^2), I^g(\sigma^1,\sigma^2), I^b(\sigma^1,\sigma^2)\right).$$

We note that there are obvious better selections to color space definition rather than the RGB flat space. Nevertheless, we get impressive results even from this oversimplified assumption.

We minimize our action (20) with respect to the metric and with respect to (I^r, I^g, I^b). For convenience we denote below (r,g,b) by $(1,2,3)$, or in general notation i. Minimizing the metric gives, as usual, the induced metric which is given in this case as follows:

$$\begin{aligned} g_{11} &= 1 + (I^1_x)^2 + (I^2_x)^2 + (I^3_x)^2, \\ g_{12} &= I^1_x I^1_y + I^2_x I^2_y + I^3_x I^3_y, \\ g_{22} &= 1 + (I^1_y)^2 + (I^2_y)^2 + (I^3_y)^2, \\ g &= \det(g_{ij}) = g_{11}g_{22} - g^2_{12}. \end{aligned}$$

Note that this metric differs from the Di Zenzo metric [15] by the addition of 1 to g_{11} and g_{22}. The source of the difference is the map used to describe the image. Di Zenzo used $X : \mathbb{R}^2 \rightarrow \mathbb{R}^3$ while we use $X : \Sigma \rightarrow \mathbb{R}^5$.

The action functional under this choice of the metric is the Euler functional

$$S = \int d^2\sigma \sqrt{g}, \tag{51}$$

where the *generalized surface area element* $\sqrt{g}$ is defined by

$$g = 1 + \sum_i |\nabla I^i|^2 + \sum_{ij} (\nabla I^i, \nabla I^j)^2,$$

where (A, B) stand for the magnitude of the vector product of the vectors A and B.

The action is simply the area of the image surface. Minimization with respect to I^i gives the Beltrami flow

$$I^i_t = \frac{1}{\sqrt{g}}\partial_\mu(\sqrt{g}g^{\mu\nu}\partial_\nu I^i). \tag{52}$$

Which is a flow towards a minimal surface.

For simple implementation of the Beltrami flow let us first compute the 6 matrices: I^i_x, I^i_y, and the following 6 matrices:

$$\begin{aligned} p^i &= \frac{g_{22}}{\sqrt{g}}I^i_x - \frac{g_{12}}{\sqrt{g}}I^i_y, \\ q^i &= -\frac{g_{12}}{\sqrt{g}}I^i_x + \frac{g_{11}}{\sqrt{g}}I^i_y. \end{aligned}$$

Then the evolution is given by

$$I^i_t = \frac{1}{\sqrt{g}}\left(p^i_x + q^i_y\right). \tag{53}$$

6.1 Relation to the color snakes and color TV

The geodesic active contours model is defined by the flow:

$$u_t = \text{div}\left(f\frac{\nabla u}{|\nabla u|}\right)|\nabla u|.$$

where f is a potential computed from the initial image, e.g. $f = 1/(1 + |\nabla I|^2)$. This is the steepest decent flow that minimizes $\int f|\nabla u|$, or equivalently any level set of u defines a curve, for which the above flow is the weighted arclength minimization flow [7, 6, 8, 25, 45]. Sapiro noted in [41] that a straight forward extension of this model to color space is by simply replacing the potential f that was extracted from a gray level image, by f_{color}, extracted from the color, or any other space. He also introduced the 'self color snakes'

$$I^i_t = \text{div}\left(f_{color}(t)\frac{\nabla I^i}{|\nabla I^i|}\right).$$

Where now $f = 1/(\lambda_+ + \lambda_-)$ is a function of the eigenvalues of the multi valued image metric [15].

Sapiro and Ringach [43, 42], and Chambolle [9], generalized the idea of smoothing a single valued function via a second directional derivative in the direction of minimal change, i.e. isophotes curvature flow, into a multi valued function. It is a flow by the second derivative in the L^1 direction of minimal change. They named it 'color diffusion'.

As pointed out in [5], for image segmentation, edge preserving and selective smoothing purposes, the 'self color snakes' is a result of a weekly coupled definition for an arclength in color space. They also claimed that from the class of all possible norms of the form $f(\lambda^+, \lambda^-)$, the $f(\lambda^+ + \lambda^-)$ is the most natural one. Blomgren and Chan [5] try to improve Sapiro's results and defined the color TV that is described bellow.

Consider an RGB color image. Let $m = 3$ color 'channels', the color TV [5] minimizes the norm:

$$\mathrm{TV}_m = \sqrt{\sum_{i=1}^{m} \left(\int |\nabla I^i| \right)^2},$$

with a constraint that yields the minimization of

$$\mathrm{TV}_m - \lambda \sum_{i=1}^{m} \int (I^i - I_0^i)^2.$$

The corresponding Euler-Lagrange equation is

$$\mathrm{div}\left(\frac{\nabla I_i}{|\nabla I_i|} \right) - \lambda_i (I_i - I_i^0) = 0,$$

where

$$\lambda_i = \lambda \frac{\mathrm{TV}_m}{\int |\nabla I^i|}.$$

Observe that in this case the coupling between the channels is only by the constraint. Actually, without the constraint the minimization yields a channel by channel curvature flow. Moreover, in order to obtain an efficient numerical scheme, Blomgren and Chan [5] regularize the TV into what we showed is a channel by channel minimal surface coupled via the constraint.

We notice that our $\int \sqrt{g}$ norm which yield a natural coupling between the channels via different geometric flow: the Beltrami flow. The Beltrami flow converges to either the TV in the 1D case as the regularization ratio β goes to zero, or to a simple heat equation in $\mathbb{R}^m$ for large β. Which means that we arrive at a 'color diffusion' or selective smoothing leading towards segmentation (under the right constraints) by just tuning the β ratio to the right value.

In the following sections we demonstrate our framework by two examples. We introduce a new segmentation scheme and present color denoising results.

7 Segmentation of Gray Level Images: Improving the Yanovitz-Bruckstein Method

In our first example, we address a simple version of the segmentation problem in which the goal is to separate objects from their background under nonuniform and poor illumination. We shall follow the steps given in [50], which yield one of the best results in recent comparison surveys. In [48, 47], Trier, Taxt, and Jain evaluate the performance of published binarization methods for document images and found that the Yanovitz-Bruckstein method performs better than most of the other algorithms, yet require high computational complexity for its main step: the generation of the threshold surface. In [50], Yanovitz and Bruckstein argue that a preferable threshold would be a minimal surface with constraints at the edges. However, they avoid computing the true minimal surface due to the numerical complexity of the non-linear equation, and preferred computing a potential surface (Gaussian filtering with constraints) and explored its direct mathematical connection to minimal surfaces.

In order to construct an efficient, as well as geometrically correct method we introduce a new algorithm for replacing the core of the Yanovitz-Bruckstein method. We use a parameterized function formulation for the mean curvature flow [35, 12] leading towards a minimal surface, to replace the computationally expensive procedure for the potential surface that was used in [50]. The new algorithm reduces the complexity of the threshold computation step and results in the correct minimal (threshold) surface for the image segmentation.

The proposed segmentation method, like the YB method, handles nonuniform illumination and noisy images for general purpose object segmentation. We have used the basic and simplest edge detectors for constructing the edge/boundary support. In general, incorporating a-priori knowledge on the problem in hand may help to achieve better performances.

7.1 The Segmentation Steps

We follow the main steps as in [50], yet now with flow towards a minimal surface based implementation.

The new segmentation process is based on 5 steps: geometric smoothing, edge extraction, minimal surface computation with constraints at the edges, subtraction of the minimal (threshold) surface from the original image, and filtering out the ghosting effects (validation). We formulate the smoothing, as well as the validation (ghosts filtering) steps as flows leading towards a minimal surface. The segmentation process is given by the following steps (see Fig. 5):

1. Smooth the original image via the Beltrami flow for a short period of time to filter out

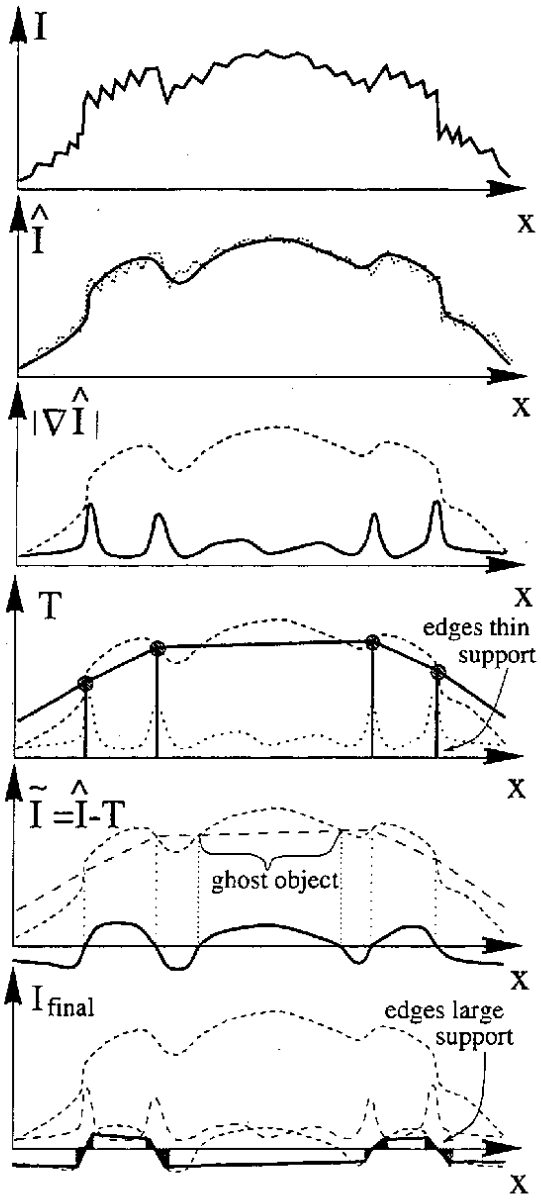

Figure 5: Description of the whole segmentation process on a 1D example, top to bottom: $I(x)$ the original noisy image. $\hat{I}$ result of Beltrami denoising. $|\nabla \hat{I}|$ the gradient magnitude of the denoised image. T the threshold minimal surface, obtained with 'thin' constraints along the edges. $\tilde{I} = \hat{I} - T$ and the 'ghost' object created in the center. I_{final} is the image after validation process: obtained as a minimal surface with large support for the constraints along the boundary (the support domain is obtained from the gradient magnitude of the smoothed original image $|\nabla \hat{I}|$).

the high frequency geometric noise (high curvature of the image surface):

$$\frac{\partial}{\partial t} I(x,y,t) = \Delta_g I(x,y,t), \tag{54}$$

with initial conditions $I(x,y,0) = I(x,y)$. Evolve the above for $t = \Delta t$, and obtain $\hat{I}(x,y) = I(x,y,\Delta t)$, a smoothed version of the original image, as an input for the next step.

2. Compute the edges of $\hat{I}(x,y)$, then use these edges to construct a binary map $B(x,y)$ for the next step where

$$B(x,y) = \begin{cases} 0 & (x,y) \in \text{edges} \\ 1 & \text{elsewhere.} \end{cases} \tag{55}$$

3. Use B as boundary conditions for computing the minimal threshold surface T. Use the smoothed image as initial conditions $I(x,y,0) = \hat{I}(x,y)$, to

$$\frac{\partial}{\partial t} I(x,y,t) = B(x,y) g \Delta_g I(x,y,t). \tag{56}$$

Let the threshold minimal surface be the solution of the above flow, i.e. $(x,y,T(x,y)) = (x,y,I(x,y,\infty))$.

4. Let $\tilde{I}(x,y) = \hat{I}(x,y) - T(x,y)$ be the segmented image.

5. We still need to get rid of the ghosting effects by a validation process. Let us again use the Beltrami flow for this purpose: Extend the zero regions of $B(x,y)$ so that these regions now support the whole edge instead of just its middle points into $\tilde{B}(x,y)$. A morphological dilation of the zero regions by one pixel is usually enough, or alternatively thresholding $|\nabla \hat{I}|$ with a low threshold. Use the result of the previous step as initial condition $I(x,y,0) = \tilde{I}(x,y)$, to the Beltrami de-ghosting/validation flow:

$$\frac{\partial}{\partial t} I(x,y,t) = \tilde{B}(x,y) \Delta_g I(x,y,t). \tag{57}$$

The result $I(x,y,\infty)$ is then thresholded (by zero) to yield the desired segmented image.

Choosing the right time step in the numerical approximation of the above flows leads to an efficient convergence in which few iterations are enough. Typically a total number of 50 iterations yield the desired result. See [10] for efficient numerical schemes like the *primal-dual Newton method.* These methods are efficient especially in the cases of given constraints or fixed boundary conditions.

7.2 Results

Figures 6 and 7 show the result of the different steps we have just described. The noise in all cases is Gaussian added to the gray level image. The variance is computed as $\sigma^2 = \int (I^{\text{original+noise}} - I^{\text{original}})^2 dxdy$. We have normalized the intensity (white = 1), in which case $\sigma = 36$ for the hand image, and $\sigma = 64$ for the map image.

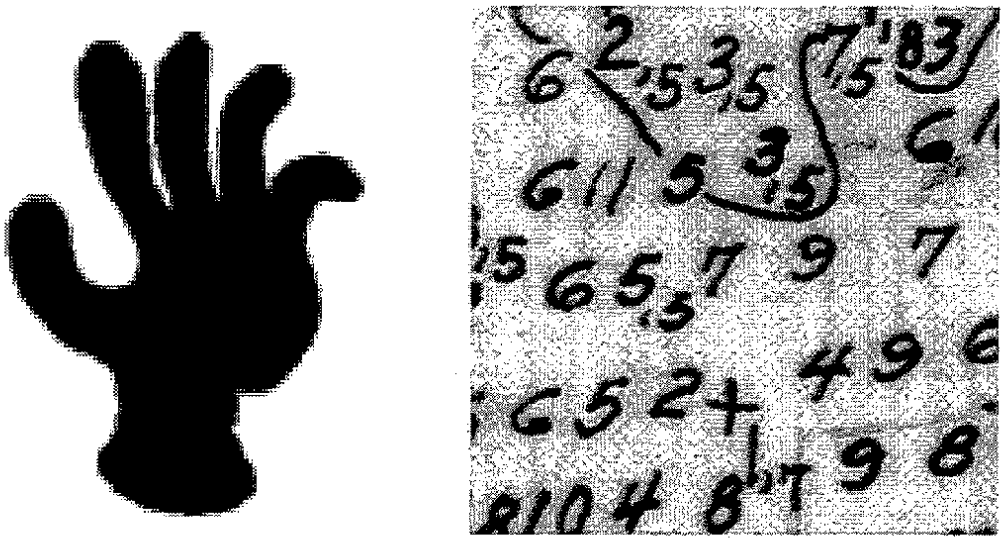

Figure 6: Original images. The hand image resolution is 128×128. The numbers image is 256×256, it is part of a scanned hydrographic map that shows depth values and contours of constant depth (obtained form O. Trier homepage). The gray level resolution is 256 and was normalized to 1, i.e. white is 1 and black is 0.

7.3 Gray level segmentation: Summary

Based on the mean curvature and the Beltrami flows with gray value constraints at the edge points, we have been able to improve the the YB segmentation method. We have formulated the whole process as a flow towards a minimal surface with and without constraints. It was shown how to use the image as initial condition to a PDE describing the mean curvature flow and the Beltrami flow (selective mean curvature flow), and how to impose the gray value constraints at the detected edges locations. This way, a minimal surface is obtained and used as the threshold surface. This is a pure geometric approach, it is invariant to translations and rotations of coordinates (invariant to the Eulerian group of transformations). The result is a simple and efficient binarization approach for poor and non-uniform illumination conditions. The extension to color images is straight forward.

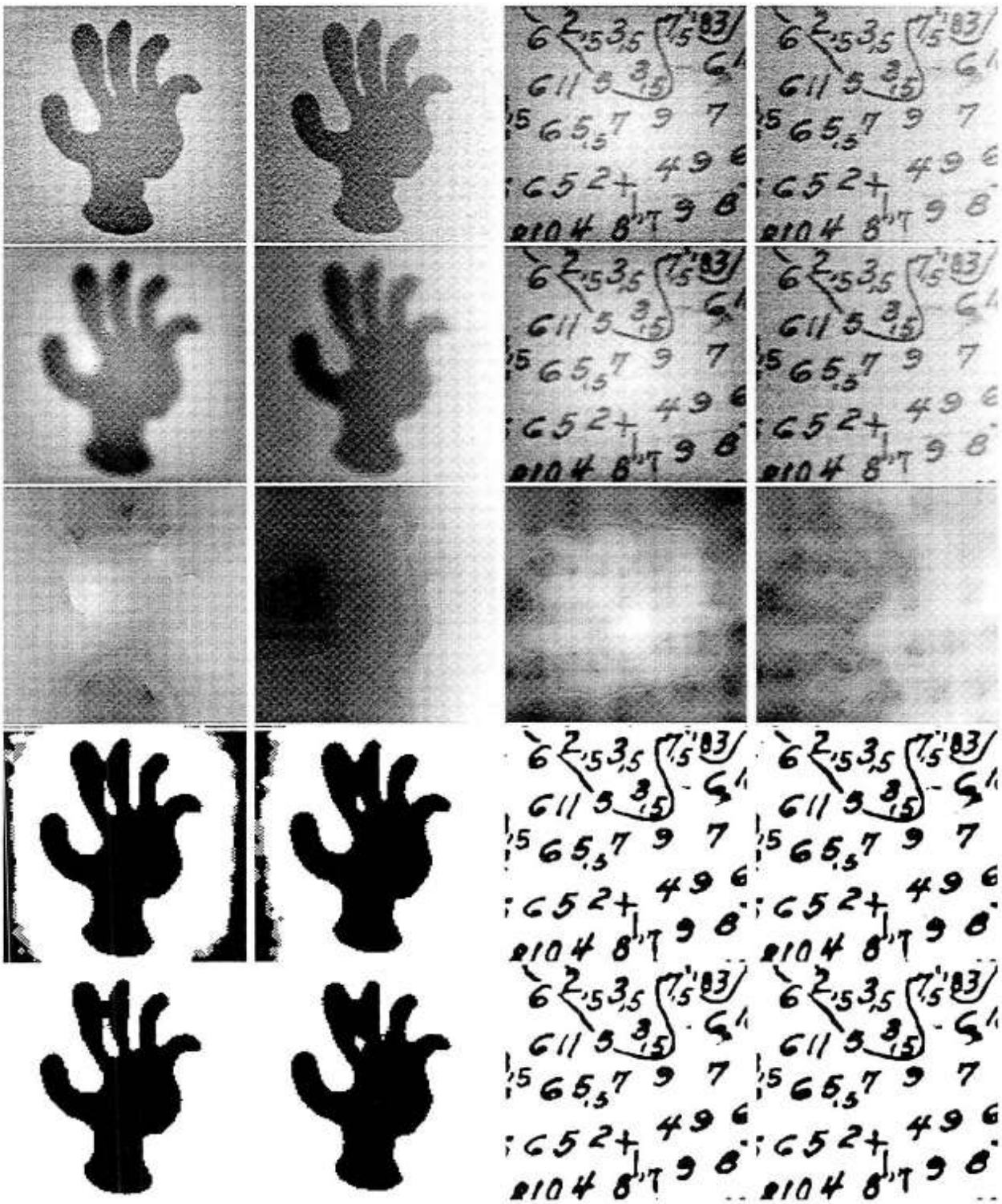

Figure 7: Rows top to bottom: 1. Original image + noise + smooth function. An intensity plane $I + x$ is added to the right, and $I + \sin(x)\sin(y)$ to the left of each pair. 2. Smoothed image. 3. Threshold surface. 4. Binarization before validation. 5. Binarization after validation.

Applying the flow towards a minimal surface with and without constraints on an image, we were able to: 1). selectively smooth the noisy image, 2). obtain a threshold surface, 3). validate the segmented regions (ghosts filtering), and together obtain a new and efficient segmentation framework.

8 Beltrami Flow in Color Space

We now present some results of denoising color images using our model. Spatial derivatives are approximated using central differences and an explicit Euler step is employed to reach the solution. We represent the image in the RGB space; however, other representations and different numerical schemes (as in [10]) are possible.

In the first example, we corrupt a given image with Gaussian noise and denoise it using our method. The left column in Fig. 8 shows two images corrupted with noise and corresponding images in the right column depict their reconstruction. In the second example, we consider noise artifacts introduced by lossy compression algorithms such as JPEG. Fig. 9(a) shows a JPEG compressed image and Fig. 9(b) its "corrected" version. The next set of figures depict two images based on wavelet compression and the corresponding reconstructed images (see Fig. 9(d) and (f)).

In Appendix B we show how to derive convergence schemes based on the Beltrami flow by adding variance constraints. However, since we have a powerful selective smoothing operator, good results may be obtained even without invoking these constraints. Without the constraints, the time we 'play' the evolution should be proportional to the noise variance.

9 Concluding Remarks

Inventing a perceptually good segmentation process, and formulating a meaningful scale space for images is not an easy task, and is actually what low level vision research is about. Here we tried to address these questions and to come up with a new framework that unifies many previous results and introduces new procedures. There are still many open questions to be asked, like what is the right aspect ratio between the intensity and the image plane? Or in a more general sense, a common and deep question that both the fields of string theory and computer vision try to answer, is what is the 'right' embedding space h_{ij}?

The question of what is the 'right norm' when dealing with images is indeed not trivial, and the right answer probably depends on the application. For example, the answer for the 'right' color metric h_{ij} is the consequence of empirical results, experimental data, and the application. Here we covered some of the gaps between the two classical norms in a geometrical way and proposed a new approach to deal with multi dimensional images. We used

(a) 50% Gaussian noise

(b) Reconstructed

(c) 100% Gaussian noise

(d) Reconstructed

Figure 8: Reconstruction of color images corrupted with Gaussian noise; we solve our scheme for 150 and 300 steps for the first and second images respectively (this is a color image).

(a) JPEG (1:10)

(b) Reconstructed

(c) Wavelet-based (1:10)

(d) Reconstructed

(e) Wavelet-based (1:20)

(f) Reconstructed

Figure 9: Reconstruction of images that are corrupted by compression algorithms such as JPEG and those that are based on wavelet transform; we run our scheme for 150 steps in each case (this is a color image).

recent results from high energy physics that yield promising algorithms for enhancement, segmentation and scale space.

Acknowledgments

We thank David Adalsteinsson of LBNL for his comments on hypersurfaces and embedding spaces, and Korkut Bardakçi for discussions on extrinsic properties of surface embedding. We thank David Marimont of XEROX PARC for supplying color images in Figs. 8(a) and 9. We thank Peter Schroeder, California Inst. Tech, for image in Fig. 8.c. This work is supported in part by the Applied Mathematics Subprogram of the Office of Energy Research under DE-AC03-76SFOOO98, ONR grant under NOOO14-96-1-0381, and in part by the National Science Foundation under grant PHY-90-21139. All calculations were performed at the Lawrence Berkeley National Laboratory, University of California, Berkeley.

Appendix A

In this appendix we derive the Euler-Lagrange equations of the Polyakov action. In order to do that let us give first some definitions and identities. First let us recall the definition of the delta function. The first thing we should know about the delta function $\delta(x-x')$ is that it is not a function. It is a distribution which can be thought of as the limit of the normal distribution, for example, when the variance goes to zero. In this limit the delta function is zero for any non zero value of the argument and infinity when the argument is zero. Formally the delta function is defined as the functional that map any function $f(x)$ to the value of the function at zero $f(0)$. In particular

$$\int dx\delta(x) = 1,$$

and in general

$$\int dx\delta(x-x')f(x) = f(x').$$

Now that we now what a delta function is we can ask what the following distribution $\frac{\partial\delta(x)}{\partial x}$ does? The answer is simple

$$\int dx\partial\delta(x)f(x) = \partial\delta(x)f(x)|_{-\infty}^{\infty} - \int dx\delta(x)\partial f(x) = -\int dx\delta(x)\partial f(x) = -\partial f(0).$$

integrating by parts we notice that the surface term vanishes because the delta function and its derivatives vanishes there.

The next piece of information needed is the variation of a function:

$$\frac{\delta f^i(x)}{\delta g^j(y)} = \delta^i_j \delta(x-y)$$

Now we can vary the action with respect to the embedding. Recall the form the form of the Polyakov action

$$S[X^i, g_{\mu\nu}, h_{ij}] = \int d^m\sigma \sqrt{g} g^{\mu\nu} \partial_\mu X^i \partial_\nu X^j h_{ij}(X)$$

The variation with respect to X^i goes as follows

$$\begin{aligned}
\frac{\delta S}{\delta X^k(\sigma)} &= \int d^m\sigma \sqrt{g} g^{\mu\nu} \partial_\mu \delta_{ik} \delta^m(\sigma-\sigma') \partial_\nu X^j h_{ij}(X) \\
&\quad + \int d^m\sigma \sqrt{g} g^{\mu\nu} \partial_\mu X^i \partial_\nu \delta_{jk} \delta^m(\sigma-\sigma') h_{ij}(X) \\
&\quad + \int d^m\sigma \sqrt{g} g^{\mu\nu} \partial_\mu X^i \partial_\nu X^j \partial_k h_{ij}(X) \delta^m(\sigma-\sigma').
\end{aligned}$$

We use now the identity we derived above

$$\begin{aligned}
\frac{\delta S}{\delta X^k(\sigma)} &= -\partial_\mu(\sqrt{g} g^{\mu\nu} \partial_\nu X^j) h_{kj}(X) - (\sqrt{g} g^{\mu\nu} \partial_\nu X^j) \partial_\mu h_{kj}(X) \\
&\quad -\partial_\nu(\sqrt{g} g^{\mu\nu} \partial_\mu X^i) h_{ik}(X) - (\sqrt{g} g^{\mu\nu} \partial_\mu X^i) \partial_\nu h_{ik}(X) \\
&\quad +\sqrt{g} g^{\mu\nu} \partial_\mu X^i \partial_\nu X^j \partial_k h_{ij}(X) \\
&= -\partial_\mu(\sqrt{g} g^{\mu\nu} \partial_\nu X^j) h_{kj}(X) - (\sqrt{g} g^{\mu\nu} \partial_\nu X^j) \partial_\mu X^i \partial_i h_{kj}(X) \\
&\quad -\partial_\nu(\sqrt{g} g^{\mu\nu} \partial_\mu X^i) h_{ik}(X) - (\sqrt{g} g^{\mu\nu} \partial_\mu X^i) \partial_\nu X^j \partial_j h_{ik}(X) \\
&\quad +\sqrt{g} g^{\mu\nu} \partial_\mu X^i \partial_\nu X^j \partial_k h_{ij}(X) \\
&= -2\partial_\mu(\sqrt{g} g^{\mu\nu} \partial_\nu X^i) h_{ik}(X) \\
&\quad -\sqrt{g} g^{\mu\nu} \partial_\mu X^i \partial_\nu X^j (\partial_i h_{kj}(X) + \partial_j h_{ik}(X) - \partial_k h_{ij}(X)).
\end{aligned}$$

From the definitions in Section 2, we end up with the desired result

$$-\frac{1}{2\sqrt{g}} h^{lk} \frac{\delta S}{\delta X^k(\sigma)} = \frac{1}{\sqrt{g}} \partial_\mu(\sqrt{g} g^{\mu\nu} \partial_\nu X^l) + \Gamma^l_{jk} \partial_\mu X^j \partial_\nu X^k g^{\mu\nu}.$$

Next we vary the Polyakov action with respect to the image metric (g_{ij}). We need the following identities:

$$\begin{aligned}
\delta g^{\mu\nu} &= -g^{\mu\kappa} \delta g_{\kappa\lambda} g^{\lambda\nu} \\
\delta g &= g g^{\mu\nu} \delta g_{\mu\nu}
\end{aligned}$$

The first identity follows from the fact that $g^{\mu\nu} g_{\nu\kappa} = \delta^\mu_\kappa$. Varying this equation we get

$$\delta g^{\mu\nu} g_{\nu\kappa} + g^{\mu\nu} \delta g_{\nu\kappa} = 0$$

and multiplying by $g^{\kappa\lambda}$ we finally obtain

$$\delta g^{\mu\nu}\delta^{\lambda}_{\nu} = \delta g^{\mu\lambda} = -g^{\mu\nu}\delta g_{\nu\kappa}g^{\kappa\lambda}$$

The secomd identity is proved using the relation

$$\log(\det(g_{\mu\nu})) = \mathrm{Tr}(\log(g_{\mu\nu}))$$

which is proved by diagonalizing $(g_{\mu\nu}) \rightarrow \begin{pmatrix} \lambda_1 & 0 \\ 0 & \lambda_2 \end{pmatrix}$ such that the relation above reads

$$\log(\lambda_1\lambda_2) = \log\lambda_1 + \log\lambda_2.$$

Varying the left hand side we have

$$\delta(\log g) = g^{-1}\delta g.$$

To vary the right hand side we need to calculate $\delta(\log(g_{\mu\nu}))$. This is done as follows

$$\delta g_{\mu\nu} = \delta(e^{\log(g_{\mu\nu})}) = \delta(\log(g_{\mu\nu}))g_{\mu\nu}$$

so that

$$\delta\mathrm{Tr}(\log(g_{\mu\nu})) = \mathrm{Tr}(\delta(\log(g_{\mu\nu}))) = g^{\mu\nu}\delta g_{\mu\nu}.$$

Now we are ready to vary the action:

$$\begin{aligned}\delta S &= \frac{1}{2\sqrt{g}}\delta g g^{\mu\nu}\partial_\mu X^i\partial_\nu X^j h_{ij}(X) + \sqrt{g}\delta g^{\mu\nu}\partial_\mu X^i\partial_\nu X^j h_{ij}(X) \\ &= \frac{1}{2}\sqrt{g}g^{\alpha\beta}\delta g_{\alpha\beta}g^{\mu\nu}\partial_\mu X^i\partial_\nu X^j h_{ij}(X) - \sqrt{g}\delta g^{\mu\kappa}\delta g_{\kappa\lambda}g^{\lambda\nu}\partial_\mu X^i\partial_\nu X^j h_{ij}(X)\end{aligned}$$

and multiplying by some factors (and summing over the indices) we obtain the result

$$-\frac{1}{\sqrt{g}}g_{\alpha\lambda}g_{\beta\kappa}\frac{\delta S}{\delta g_{\alpha\beta}} = \partial_\lambda X^i\partial_\kappa X^j h_{ij}(X) - \frac{1}{2}g_{\lambda\kappa}g^{\mu\nu}\partial_\mu X^i\partial_\nu X^j h_{ij}(X)$$

Appendix B: Constraints on Beltrami Flow

It is possible to impose a meaningful convergence on the Beltrami flow through the right constraints on the action functional. As a simple example we derive a variance constraint similar to the TV method [40] for image denoising with convergence.

We introduce two alternatives for the variance constraint. The first is the variance given for every channel, i.e.

$$\int (I^i - I^i_0)^2 dxdy = \sigma_i^2 \tag{58}$$

where here σ_i is the given noise variance for channel i. The Euler Lagrange is given by

$$\sum_{\alpha=x,y} \frac{1}{2}\partial_\alpha \left(\frac{1}{\sqrt{g}} \frac{\partial g}{\partial I^i_\alpha} \right) - \lambda^i (I^i - I^i_0) = 0. \tag{59}$$

Again, using our freedom for the selection of the parametrization (multiplying by $g^{-1/2}$), yields the flow

$$I^i_t = \Delta_g I^i - \frac{1}{\sqrt{g}} \lambda^i (I^i - I^i_0), \tag{60}$$

where λ^i is computed via

$$\lambda^i = -\frac{1}{2\sigma_i^2} \int \sum_{\alpha=x,y} \frac{1}{\sqrt{g}} \frac{\partial g}{\partial I^i_\alpha} (I^i_\alpha - I^i_{0\alpha}) dx dy. \tag{61}$$

In the second case the variance is given for all channels, i.e.

$$\sum_i \int (I^i - I^i_0)^2 dx dy = \sigma^2. \tag{62}$$

The Euler Lagrange is given by

$$\sum_{\alpha=x,y} \frac{1}{2}\partial_\alpha \left(\frac{1}{\sqrt{g}} \frac{\partial g}{\partial I^i_\alpha} \right) - \lambda (I^i - I^i_0) = 0. \tag{63}$$

That after normalization by the metric yields the flow

$$I^i_t = \Delta_g I^i - \frac{1}{\sqrt{g}} \lambda (I^i - I^i_0), \tag{64}$$

where λ is computed via

$$\lambda^i = -\frac{1}{2\sigma^2} \sum_{i=1,2,3} \int \sum_{\alpha=x,y} \frac{1}{\sqrt{g}} \frac{\partial g}{\partial I^i_\alpha} (I^i_\alpha - I^i_{0\alpha}) dx dy. \tag{65}$$

In both cases we have used the notation $\partial g / \partial I^i_\alpha$, that for the color case simplifies to

$$\frac{\partial g}{\partial I^i_x} = 2 I^i_x g_{22} - 2 I^i_y g_{12}, \qquad \text{and} \qquad \frac{\partial g}{\partial I^i_y} = 2 I^i_y g_{11} - 2 I^i_x g_{12}. \tag{66}$$

Where for color $i = 1, 2, 3$.

References

[1] L Alvarez, F Guichard, P L Lions, and J M Morel. Axioms and fundamental equations of image processing. *Arch. Rational Mechanics*, 123, 1993.

[2] L Alvarez, P L Lions, and J M Morel. Image selective smoothing and edge detection by nonlinear diffusion. *SIAM J. Numer. Anal*, 29:845–866, 1992.

[3] L Alvarez and J M Morel. Morphological approach to multiscale analysis: From principles to equations. In B M ter Haar Romeny, editor, *Geometric-Driven Diffusion in Computer Vision*. Kluwer Academic Publishers, The Netherlands, 1994.

[4] A Blake and A Zisserman. *Visual Reconstruction*. MIT Press, Cambridge, Massachusetts, 1987.

[5] P Blomgren and T F Chan. Color TV: Total variation methods for restoration of vector valued images. cam TR, UCLA, 1996.

[6] V Caselles, R Kimmel, and G Sapiro. Geodesic active contours. In *Proceedings ICCV'95*, pages 694-699, Boston, Massachusetts, June 1995.

[7] V Caselles, R Kimmel, and G Sapiro. Geodesic active contours. *IJCV*, to appear, 1995.

[8] V Caselles, R Kimmel, G Sapiro, and C Sbert. Minimal surfaces: A geometric three dimensional segmentation approach. *Numerische Mathematik*, to appear, 1996.

[9] A Chambolle. Partial differential equations and image processing. In *Proceedings IEEE ICIP*, Austin, Texas, November 1994.

[10] T F Chan, G H Golub, and P Mulet. A nonlinear primal-dual method for total variation-based image restoration. *Presented at AMS/SIAM workshop on Linear and Nonlinear CG methods*, July 1995.

[11] D L Chopp. Computing minimal surfaces via level set curvature flow. Ph.D Thesis, Lawrence Berkeley Lab. and Dep. of Math. LBL-30685, Uni. of CA. Berkeley, May 1991.

[12] D L Chopp. Computing minimal surfaces via level set curvature flow. *J. of Computational Physics*, 106(1):77–91, May 1993.

[13] D L Chopp and J A Sethian. Flow under curvature: Singularity formation, minimal surfaces, and geodesics. *Jour. Exper. Math.*, 2(4):235–255, 1993.

[14] P Concus. Numerical solution of the minimal surface equation. *Mathematics of Computation*, 21:340–350, 1967.

[15] S Di Zenzo. A note on the gradient of a multi image. *Computer Vision, Graphics, and Image Processing*, 33:116–125, 1986.

[16] B A Dubrovin, A T Fomenko, and S P Novikov. *Modern Geometry - Methods and Applications I.* Springer-Verlag, New York, 1984.

[17] L P Eisenhart. *Differential Geometry.* Princeton Univ. Press, Princeton, 1940.

[18] A I El-Fallah, G E Ford, V R Algazi, and R R Estes. The invariance of edges and corners under mean curvature diffusions of images. In *Processing III SPIE*, volume 2421, pages 2–14, 1994.

[19] L C Evans and J Spruck. Motion of level sets by mean curvature, I. *J. Diff. Geom.*, 33, 1991.

[20] L M J Florack, A H Salden, , B M ter Haar Romeny, J J Koendrink, and M A Viergever. Nonlinear scale-space. In B M ter Haar Romeny, editor, *Geometric–Driven Diffusion in Computer Vision.* Kluwer Academic Publishers, The Netherlands, 1994.

[21] L M J Florack, B M ter Haar Romeny, J J Koenderink, and M A Vierever. General intensity transformations and differential invariants. *Journal of Mathematical Imaging and Vision*, 4:171–187, 1994.

[22] M B Green, J H Schwarz, and E Witten. *Superstring Theories*, volume I and II. Cambridge Univ. Press, Cambridge, 1987.

[23] W E L Grimson. *From images to surfaces.* MIT Press, Cambridge, USA, 1981.

[24] H W Guggenheimer. *Differential Geometry.* McGraw-Hill Book Company, New York, 1963.

[25] S Kichenassamy, A Kumar, P Olver, A Tannenbaum, and A Yezzi. Gradient flows and geometric active contour models. In *Proceedings ICCV'95*, Boston, Massachusetts, June 1995.

[26] R Kimmel. Intrinsic scale space for images on surfaces: The geodesic curvature flow. LBNL Report LBNL 39172, LBNL UC Berkeley, CA 94720, August 1996.

[27] E Kreyszing. *Differential Geometry.* Dover Publications, Inc., New York, 1991.

[28] J L Lagrange. *Essai d'une nouvelle méthode pour déterminer les maxima et les minima des formules intégrales indéfinies*, volume I. Gauthier-Villars, Paris, 1867. translated by D. J. Struick.

[29] R Malladi and J A Sethian. Image processing: Flows under min/max curvature and mean curvature. *Graphical Models and Image Processing*, 58(2):127–141, March 1996.

[30] D Marr. *Vision*. Freeman, San Francisco, 1982.

[31] D Mumford. Bayesian rationale for the variational formulation. In B M ter Haar Romeny, editor, *Geometric–Driven Diffusion in Computer Vision*. Kluwer Academic Publishers, The Netherlands, 1994.

[32] D Mumford and J Shah. Boundary detection by minimizing functionals. In *Proceedings of CVPR, Computer Vision and Pattern Recognition*, San Francisco, 1985.

[33] M Nakahara. *Geometry, Topology and Physics*. Adam Hilger, New York, 1990.

[34] V Oliker. Self-similar solutions and asymptotic behavior of flows of nonparametric surfaces driven by the Gauss or mean curvature. In *Proceedings of Symposia in Pure Mathematics*, volume 54, pages 389–402, Part 1, 1993.

[35] S J Osher and J A Sethian. Fronts propagating with curvature dependent speed: Algorithms based on Hamilton-Jacobi formulations. *J. of Comp. Phys.*, 79:12–49, 1988.

[36] P Perona and J Malik. Scale-space and edge detection using anisotropic diffusion. *IEEE-PAMI*, 12:629–639, 1990.

[37] P Perona, T Shiota, and J Malik. Anisotropic diffusion. In B M ter Haar Romeny, editor, *Geometric–Driven Diffusion in Computer Vision*. Kluwer Academic Publishers, The Netherlands, 1994.

[38] A M Polyakov. *Physics Letters*, 103B:207, 1981.

[39] T Richardson and S Mitter. Approximation, computation, and distoration in the variational formulation. In B M ter Haar Romeny, editor, *Geometric–Driven Diffusion in Computer Vision*. Kluwer Academic Publishers, The Netherlands, 1994.

[40] L Rudin, S Osher, and E Fatemi. Nonlinear total variation based noise removal algorithms. *Physica D*, 60:259–268, 1992.

[41] G Sapiro. Vector-valued active contours. In *Proceedings IEEE CVPR'96*, pages 680–685, 1996.

[42] G Sapiro and D Ringach. Anisotropic diffusion of multivalued images. In *12th Int. Conf. on Analysis and Optimization of Systems: Images, Wavelets and PDE'S*, Paris, June 1996. Springer Verlag.

[43] G Sapiro and D L Ringach. Anisotropic diffusion in color space. *IEEE Trans. Image Proc.*, to appear, 1996.

[44] G Sapiro and A Tannenbaum. Affine invariant scale–space. *International Journal of Computer Vision*, 11(1):25–44, 1993.

[45] J Shah. A common framework for curve evolution, segmentation and anisotropic diffusion. In *Proceedings IEEE CVPR'96*, pages 136–142, 1996.

[46] D Terzopoulos. Multilevel computational processes for visual surface reconstruction. *Computer Vision Graphics and Image Processing*, 24:52–96, 1983.

[47] O D Trier and A K Jain. Goal-directed evaluation of binarization methods. *IEEE Trans. on PAMI*, 17(12):1191–1201, 1995.

[48] O D Trier and T Taxt. Evaluation of binarization methods for ducument images. *IEEE Trans. on PAMI*, 17(3):312–315, 1995.

[49] R Vogel and M E Oman. Iterative methods for total variation denoising. *SIAM. J. Sci. Statist. Comput.*, to appear, 1996.

[50] S D Yanowitz and A M Bruckstein. A new method for image segmentation. *Computer Vision, Graphics, and Image Processing*, 46:82–95, 1989.

Ernest Orlando Lawrence Berkeley National Laboratory
One Cyclotron Road | Berkeley, California 94720

Prepared for the U.S. Department of Energy under Contract No. DE-AC03-76SF00098